Plasticity-Induced Bending Of Aluminum-Polymer Layered Composites

by

Chien Nguyen

B. Sc in ME, Karlsruhe Institute of Technology, 2020

Submitted to the Graduate Faculty of the

Swanson School of Engineering in partial fulfillment

of the requirements for the degree of

Master of Science in Mechanical Engineering

University of Pittsburgh

2023

UNIVERSITY OF PITTSBURGH

SWANSON SCHOOL OF ENGINEERING

This thesis was presented

by

Chien Nguyen

It was defended on

April 7, 2023

and approved by

Jeffrey Vipperman, PhD, Professor, Mechanical and Materials Science Engineering Department

Patrick Smolinski, PhD, Associate Professor, Mechanical and Materials Science Engineering Department

Matthew Barry, PhD, Assistant Professor, Mechanical and Materials Science Engineering Department

Thesis Advisor:
Sachin Velankar, PhD, Professor, Chemical and Petroleum Engineering Department

Plasticity-Induced Bending Of Aluminum-Polymer Layered Composites

Chien Nguyen, B.Sc.

University of Pittsburgh, 2023

Deformation induced strain mismatch refers to the phenomenon where different materials bonded to each other experience different levels of inelastic deformation when subjected to external stress. This difference in deformation induces a strain mismatch, which can then cause permanent deformation of the composite. This thesis examines bilayered composites subjected to tensile stress which induces inelastic deformation in one of the layers. The resulting strain mismatch causes the bilayer system to bend when the stress is released. The resulting bending can have important implications for the mechanical behavior of multilayered thin films as well as for applications such as sensors or actuators. Understanding the factors that influence deformation induced strain mismatch and the resulting bending is therefore critical for the design and optimization of such systems.

Experiments are conducted on layered composites of soft aluminum foil and commercial polymer laminating film. Bilayers were manufactured by cold lamination, then cut into strips, and stretched to induce inelastic deformation. The bilayer strips were then unloaded from various strains and observed to bend. The bending curvature was quantified and found to increase almost linearly with the applied strain. The bending was found to reduce with increasing aluminum thickness, and to be insensitive to sample width. Aluminum-polymer bilayers that used thin foils of aluminum undergo localized delamination which relieve strain mismatch in their vicinity and therefore suppresses bending.

By patterning the bilayers, bending can be localized only at specific "defect" sites. Such defects were created by laser-ablation of the polymer. Simple trenches were made with different angles in respect to the pulling direction, or different width. When stretched and released, such composites show spatially-heterogeneous bending. Complex 3D shapes can be made by combining trenches or cutouts.

Table of Contents

Preface

I am filled with gratitude and appreciation, and I would like to express my heartfelt thanks to my advisor, Professor Sachin Velankar, for his invaluable support and guidance throughout the duration of this project. His unwavering commitment to my success and his willingness to provide me with the tools and resources necessary for the completion of this project has been immeasurable.

Furthermore, I extend my thanks to my colleague, Fatemeh, for her unwavering support and contributions to this project.

I would like to acknowledge the National Science Foundation (NSF) for providing me with the necessary funding to pursue this project. Their financial support has been a critical component in enabling me to conduct the research and experiments that formed the basis of this thesis.

In addition, I am grateful to Andy Holmes and Brandon Barber for granting me access to the laser cutter in the SCPI, and to Charles "Scooter" Hager for allowing me to use the tensile machine. Without their generous support and assistance, this project would not have been possible.

Moreover, I would like to express my gratitude to Dr. Abramowitch for allowing me to use the tensile testing equipment, which played a crucial role in the completion of this project.

Finally, I dedicate this thesis to my beloved parents, whose unwavering love, support, and encouragement have been a constant source of strength and inspiration throughout my studies. I am also grateful to my brother, whose constant nagging and motivation have helped me to remain focused and committed to this project.

1.0 Introduction

Origami, the Japanese art of paper folding, has fascinated people for centuries, and the author, with its intricate designs and elegant shapes. In recent years, origami has emerged as a rich source of inspiration for researchers in various fields, ranging from engineering and physics to biology and medicine (Peraza-Hernandez et al., 2014; Ji et al., 2021; Meloni et al., 2021; Li et al., 2023). With the advent of advanced computational tools and materials, scientists are now able to create and explore new origami-inspired structures that have potential applications in areas such as space exploration, architecture, drug delivery, and robotics (Turner et al., 2016; Webb et al., 2016; Johnson et al., 2017; Pesenti et al., 2018; Masana et al., 2020; Meloni et al., 2021). This has led to a surge in origami research, with new developments and breakthroughs being reported regularly in delivery and packaging sector (Myer et al., 1969; Konings et al., 2001; Tremblay et al., 2007; Wu et al., 2011); in manufacturing (Judy et al., 1997; Sreetharan et al., 2012); in structure (Tachi, 2010).

One development in this regard is described as "self-folding origami", or "stimulus-responsive origami" (Tolley et al., 2014; Janbaz et al., 2016; Santangelo, 2017; Stern et al., 2017). Here a flat sheet is patterned in some manner which induces local bending when exposed to some stimulus such as change in temperature, pH, solvent conditions, or electrochemical changes. Typically, the stimulus induces selective expansion of a region (or layer) of the sheet. This creates residual stress within the sheet which induces bending. The bending may be highly localized giving the appearance of the sharp folds of origami (Smela et al., 1995; Na et al., 2015), or they may be

1

more gradual changes in curvature over larger regions (Kim et al., 2012). In this thesis, we consider applied stress itself as a stimulus to induce residual stresses as explained in the next paragraph.

One interesting approach to self-folding origami is the combination of elastic and inelastic (i.e. plastic) material into a composite, and its ability to shapeshift by applying stress and then releasing (Kanik et al., 2019; Wisinger et al., 2019). The author's research group has previously worked on a rubber-plastic composite with interesting results (Ramachandran et al., 2018; Ramachandran et al., 2021). In this study, rubber-plastic bilayers were stretched and released. The plastic deforms permanently while the rubber deforms elastically. The resultant strain mismatch, namely deformation-induced mismatch due to the nature of stretched samples, gives the composite complex shapes changes when released. For example, these bilayers form helical shapes at small width or thickness, and the curvature sign changes beyond a certain strain threshold.

The objective of this research is to explore metal-polymer composites as an origami medium. Before proceeding, we clarify the nomenclature. Unlike rubber-plastic composites where plastic, like its name, went into plastic deformation, in metal-plastic composites, the metal will go into plastic deformation at very low strain. At such small strains, the "plastic" will behave elastically. To avoid confusion, we will use "metal-polymer" to refer to this material combination.

The following objectives are set for this project: firstly, to develop a rapid prototyping platform that can efficiently manufacture aluminum-polymer layered composites in meter-scale lengths to allow large-scale morphing structures; secondly, to investigate the fundamental mechanics of aluminum-polymer bilayers to enhance our understanding of how bending can be controlled by their geometry and by the applied deformation; thirdly, to devise a method to generate defect patterns so that straight strips can be "programmed" to bend into the desired shape after a being loaded and then unloaded.

1.1 Mechanics Of Elastic-Elastic Bilayer

The phenomenon of elastic bending of layered composite materials has been extensively researched and analyzed, with the bimetallic strip serving as a classic example. This strip is composed of two thin metal strips that are bonded together that have different thermal expansion coefficients. When exposed to heat, one strip expands more than the other, causing a "strain mismatch", which induces the composite to bend. As long as the strain mismatch is small enough that both layers remain elastic, the situation is well captured by existing models (Stoney, 1909; Freund et al., 2004).

Stoney (1909) found that a copper protective layer electrodeposited on silver films in searchlight reflectors easily detached when the copper layer exceeded 10 μm thickness. Stoney calculated the curvature κ of a film-substrate bilayer system with an infinitely thin film layer as

$$\kappa = \frac{6f}{E_s h_s^2} \tag{1.1}$$

with f as the membrane force that is a system parameter determined by the strain mismatch alone, E_s and h_s are the elastic modulus and thickness of the substrate, respectively. Since the film is treated as infinitely thin, the only resistance to bending comes from the substrate. The effect of the strain mismatch is then treated as a force on one of the surfaces of the substrate. Figure 1 illustrates the model of this system.
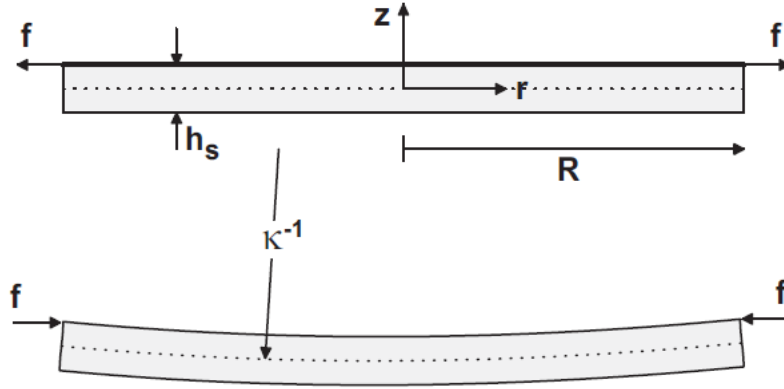
Figure 1: Stoney's bilayer system with thin film on a thick substrate and the resulted curvature (Freund & Suresh, 2004).

Due to Stoney method's assumptions, the strain mismatch and film properties do not appear explicitly, and the equation is only valid when the substrate is much thicker than the film. Freund et al. (1999) conducted a more detailed analysis later and accounted for finite film thickness and generalized Stoney's equation for arbitrary thickness ratio and arbitrary modulus ratio:

$$\frac{\kappa}{\kappa_{St}} = \left(1 + \frac{h_f}{h_s}\right)\left[1 + 4\frac{h_f}{h_s}\frac{E_f}{E_s} + 6\frac{h_f^2}{h_s^2}\frac{E_f}{E_s} + 4\frac{h_f^3}{h_s^3}\frac{E_f}{E_s} + \frac{h_f^4}{h_s^4}\frac{E_f^2}{E_s^2}\right]^{-1} \tag{1.2}$$

This model is illustrated in Fig. 2. The film's parameters E_f and h_f allow the calculation of κ for arbitrary material selection. The factor

$$\kappa_{St} = \frac{6\epsilon_m}{h_s}\frac{h_f}{h_s}\frac{E_f}{E_s} \tag{1.3}$$

is the curvature from Stoney's equation (obtained by replacing f with $\epsilon_m E_f h_f$), which present the loading with strain mismatch ϵ_m instead of an external force f. The curvature value κ will become this κ_{St}, when the film thickness h_f approaches zero. The curvature κ can be calculated directly from the strain mismatch and material parameters as

4

$$\kappa = \frac{6\epsilon_m}{h_s} \frac{h_f}{h_s} \frac{E_f}{E_s} \left(1 + \frac{h_f}{h_s}\right) \left[1 + 4\frac{h_f}{h_s}\frac{E_f}{E_s} + 6\frac{h_f^2}{h_s^2}\frac{E_f}{E_s} + 4\frac{h_f^3}{h_s^3}\frac{E_f}{E_s} + \frac{h_f^4}{h_s^4}\frac{E_f^2}{E_s^2}\right]^{-1} \tag{1.4}$$
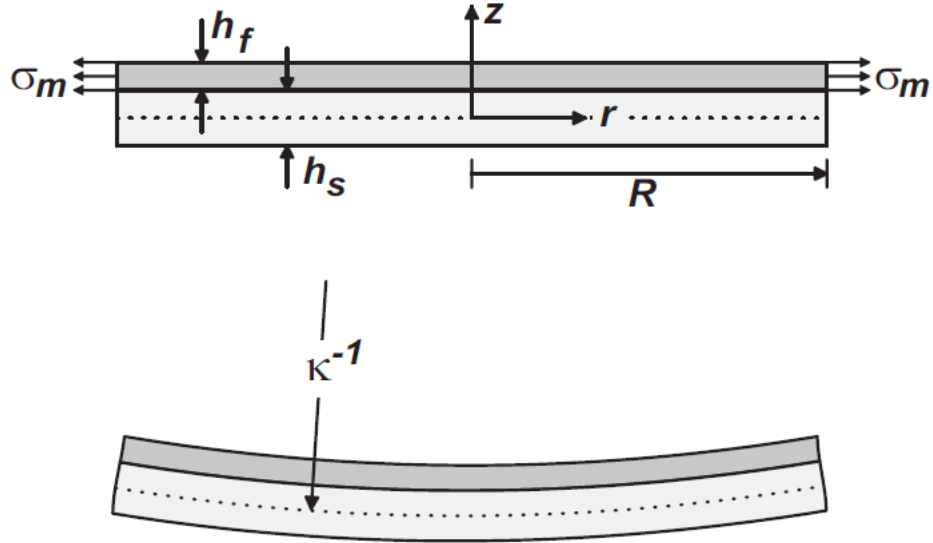
Figure 2: Bilayer system with arbitrary thickness ratio and uniform applied strain (Freund & Suresh, 2004).

It is notable that the equation above was meant to calculate the curvature for a bilayer system with elastic strain mismatch. Accordingly, it is only permissible to apply this equation for our deformation-induced strain mismatch, under the condition that aluminum remains within its elastic limit after release.

1.2 Mechanics Of Elastic-Plastic Bilayer

Suresh et al. (1994) extended the analysis of the bilayer into the plastic realm with a model of a bilayer system that consists of an elastic substrate and elastic-ideally plastic film, which have different linear thermal expansion coefficient. The strain mismatch is induced by heat. Before yielding, the curvature is similar to the Eq. (1.4). The flow stress or uniaxial yield of the film layer σ_{Y_f} can be expressed as the plastic yielding condition of the film. The film first yields at the plastic-elastic interface when the curvature reaches a value curvature κ_Y given by:

$$\kappa_Y = \frac{6\sigma_{Y_f}}{h_s E_f} \frac{h_f}{h_s} \frac{E_f}{E_s} \left(1 + \frac{h_f}{h_s}\right) \left[1 + 3\frac{h_f^2}{h_s^2}\frac{E_f}{E_s} + 4\frac{h_f^3}{h_s^3}\frac{E_f}{E_s}\right]^{-1} \tag{1.5}$$

With increasing strain mismatch, the yielding progresses throughout the film thickness, and the distribution of the stress in the film becomes uniform. Beyond this point, the curvature no longer increases with strain mismatch and saturates at the value κ_{pl}

$$\kappa_{pl} = \frac{6\sigma_{Y_f}}{h_s E_f} \frac{h_f}{h_s} \frac{E_f}{E_s} \left(1 + \frac{h_f}{h_s}\right) \tag{1.6}$$

The model assumed that the response of the film material is independent of the flow stress on temperature, and as a result the curvature κ_{pl} remains unchanged during further increase of temperature. Once the film becomes fully plastic, substrate bending and plastic yielding in the film are exhausted and any further change in thermal strain mismatch is accommodated by the in-plane extensional strain. For a deformation-induced strain mismatch bilayer system, it is difficult to verify quantitatively whether the film yields when release, but this analysis can be used as guidance.

1.3 Large Deformation Bilayer

At large deformations, some bilayer systems develop complex shape changes that are non-intuitive. For example, Ramachandran et al. (2021) showed rubber-plastic samples that formed arches at small strain, saddles at intermediate strain, and tubes at large strain. Going from small to large strain, the direction and sign of the curvature both flip, and wrinkles formed in the plastic layer:
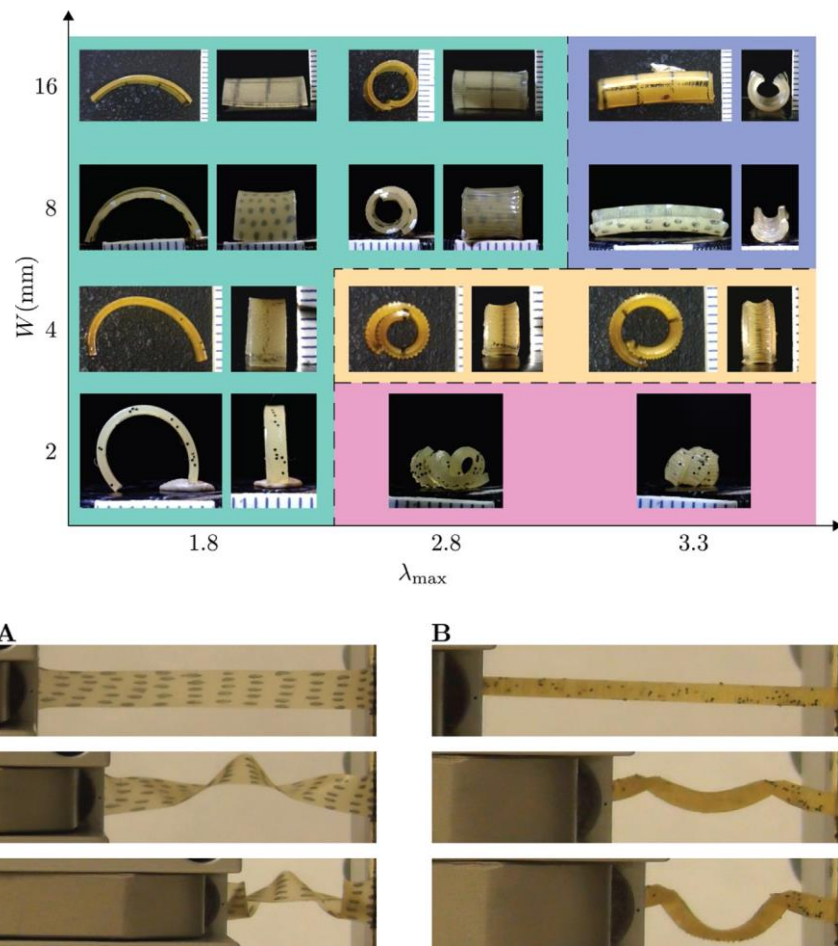
Figure 3: Rubber-plastic bilayer forms complex shapes. Top: changes with different levels of maximum strain and sample width. Bottom: helixes formed in small width sample with end constraints (Ramachandran et al., 2021).

Similar to these non-intuitive shape changes, Wisinger et al. (2019) experimented on stretch-and-released elastomers bilayer and recognized different output shapes based on bilayer aspect ratio and applied strain: bends, curling, twisting into helix and rolling into a cylinder. Kanik et al. (2019) used a bimorph fiber system as a bilayer and a heating-drawing process with strain up to 1,300 % to generate spring-like actuators.

In most of this thesis, such unexpected shape changes do not appear. However, at high strain, metal-polymer bilayer can also develop unexpected shape changes due to end constraints. We will discuss this in Section 3.3.2.

The main objective of this thesis is to create a metal-polymer composite of large length and study its bending mechanics. This study represents the first investigation of a metal-polymer composite with deformation-induced mismatch, which can result from the interplay of plastic and elastic deformation. The research also aims to develop methods for patterning the composite material. One of the primary questions addressed in this study is whether the existing theory for elastic bilayer can be applied to capture deformation-induced mismatch in the metal-polymer composite. Through this research, the hope is to gain a better understanding of the behavior of metal-polymer composites and contribute to the development of new materials with unique properties for various engineering applications.

2.0 Materials And Experimental Methods

Composite samples were created using an office cold laminator to laminate thin aluminum sheet on both sides with polymer sheets pre-applied with pressure sensitive adhesive. By coating one surface of the aluminum with oil, it is then possible to peel off the polymer layer easily to obtain aluminum-polymer bilayers. FTIR spectroscopy suggests that the polymer is polyethylene terephthalate (PET). By dissolving the adhesive, this polymer layer thickness can be measured to be 50 μm.

Multiple aluminum thickness from McMaster and Framar as well as kitchen grade foil was used as the metal layer. Different grades of aluminum, or different alloy types have stark differences in yield strength. For example, untempered 1100 aluminum has 24.1 MPa yield strength, while 6061 T4 aluminum has a yield strength of 110 MPa (Engineering ToolBox, 2008). To ensure the success of this research, we opted for relatively soft grades of metal, with 1000 grade aluminum from McMaster being the preferred choice. The plastic deformation of the metal plays a critical role in this study, and the selected aluminum grade was deemed appropriate for achieving the desired results.

Tensile tests were performed using MTS Equipment Tensile Machine. Strips of the laminated aluminum of widths from 4 mm to 12 mm were clamped pneumatically with a clamp-to-clamp distance of 80 mm. A preload of 0.2 N was applied on all samples to ensure that samples remained taut before stretching. Then the samples were stretched at a rate of 1 mm/min to a preset load or elongation. The maximum strain, or applied strain reached at this load or elongation is named ϵ_{max}. From this point, the samples were unloaded at the same speed until the force dropped

9

below a threshold of 0.5 N. Typically, each test was done at least 3 times and each measurement is shown individually in all graphs.

2.1 Material Selection Guided By Bilayer Mechanics

The relative thickness of the layers plays an important role determining the curvature in response to strain mismatch. If either layer is very thick, the bending of the composite reduces. This is because there is a trade-off between the thickness ratio and the resulting curvature. The thicker the film is, the more it will resist the bending and therefore the curvature will reduce. As the thickness of the film decreases, the curvature increases also, until a point where the film becomes weaker against the elastic recoil of the substrate, and therefore lowers the curvature. It is intuitively obvious that when either of the two layers becomes very thin, there will be little or no bending because the thin layer will be unable to develop sufficient stress to force the thick layer into bending. By implication, there must be a maximum bending at some value of thickness ratio.

To obtain quantitative guidance, we estimate the effect of film thickness on the curvature using an arbitrary strain mismatch of 0.15 % and equations (1.4) and (1.5). The Young's modulus for the aluminum and polymer are assumed to be 270 GPa and 1.3 GPa (see Section 3.1), respectively. The substrate, or polymer thickness is fixed at 50 μm and aluminum film thickness ranges from 0.5 to 100 μm. The results (Fig. 4) in blue show that there is an optimal aluminum thickness of 4 μm that would produce a maximum curvature. In the same figure, the vertical lines depicted the aluminum thicknesses we used, from left to right: 16, 25, 50 and 100 μm. This guides

our material selection. It clearly shows that the thinnest aluminum film would give the greatest

bending. However, the thinnest films are relatively difficult to handle and tend to crumple readily.

Accordingly, there is a tradeoff between ease of handling and the curvature expected. Practically

we found (data shown later) that aluminum thickness of 100 μm gave relatively little bending.
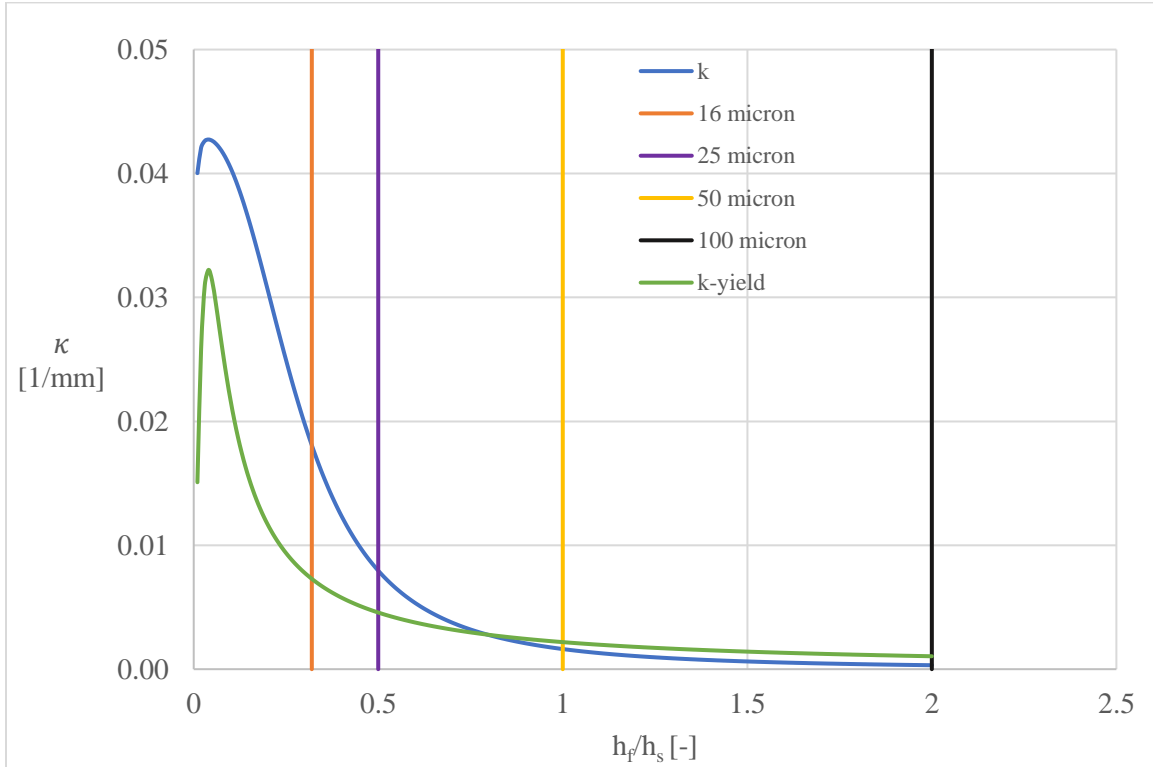
Figure 4: Effect of thickness ratio on curvature. Blue: curvature calculated from Eq. (1.4) representing an elastic-elastic bilayer system using a strain mismatch value of 0.0015. Green: curvature from Eq. (1.5) representing an elastic-ideally plastic bilayer system at first yield. Vertical lines: thickness ratio from selected aluminum thickness; from left to right: 16, 25, 50 and 100 micron aluminum.

2.2 Manufacturing Methods

Figure 5: The ezLaminator ("Xyron 9" ezLaminator,").

As mentioned above, the samples were prepared with an office "cold laminator". The laminator comes with a cartridge that has two rolls of adhesive-coated polymer sheet. The thickness of the polymer sheet was 50 μm as mentioned above. The core aluminum sheet is fed through and by turning the crank, two spring-loaded rollers press the polymer sheet onto the core sheet. It is notable that for thin materials like aluminum with a high chance of distortion or creasing during handling, alignment of the core sheet is crucial to ensure a smooth result.
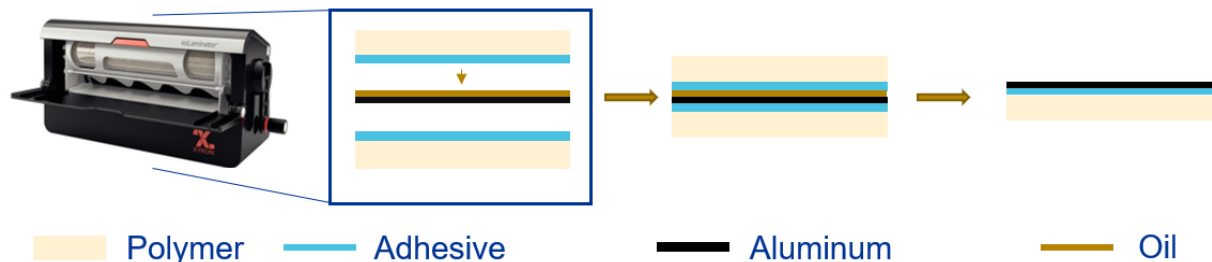
Figure 6: Schematic of manufacturing process of the bilayer.

All samples start as a trilayer by feeding an aluminum sheet through the laminator, then are cut with a laser and trimmed to size. Bilayer samples are fabricated by spraying a thin layer of cooking oil on one side of the aluminum sheet to prevent the adhesive sticking. Example of an aluminum sheet being made is shown in Fig. 7.

Figure 7: During lamination. Left: aluminum sheet being fed into back of the laminator. Right: laminated aluminum coming out in front of the laminator.

To create bilayer region on a trilayer sample, a laser cutter (RL-80-1290) was used which can change power and speed setting as well as a continuous or pulse mode. Furthermore, the laser cutter has good precision to ensure sample reproducibility. Using the laser cutter has some advantages in comparison to other subtraction methods: aluminum can reflect most of the laser for a certain range of wavelengths, so all the polymer on one side could be removed completely without permeation of damage to the other side. Too much laser power or too low speed can lead

to heat buildup and melt the polymer on the other side, while weak settings produce incomplete removal of the polymer. To prevent this, laser power and cut speed were varied at the same time to cut rectangular areas, which can be seen in Fig. 8. Numbers above the rectangular regions denote laser power in percentage of 80 W maximum power, and the numbers below it denote cut speed in mm/s. The optimal setting was found at 15 % laser and 150 mm/s, or similar result can be achieved at 20% laser power and 200 mm/s. At these settings, polymer is removed completely from one side and the back side has no visible damage.
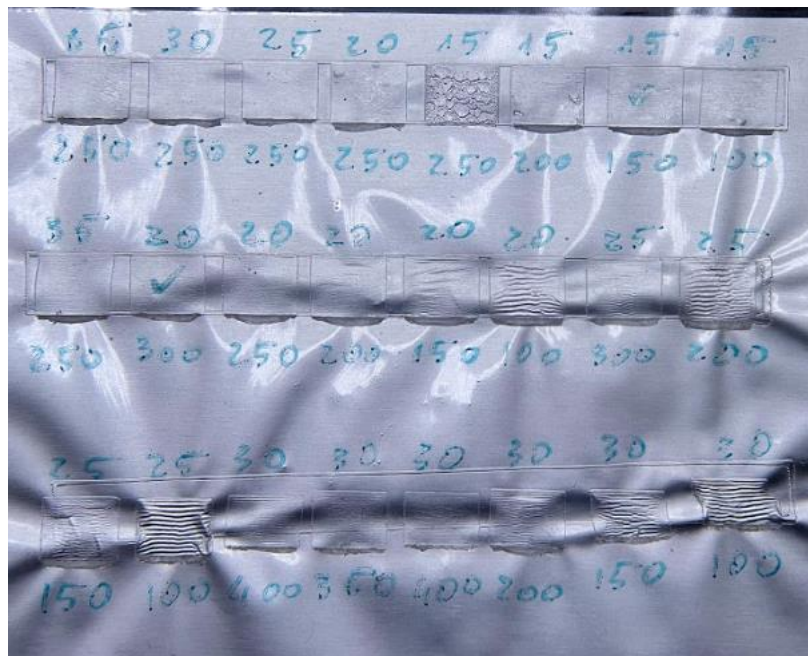
Figure 8: Effect of laser power and speed settings on removal of polymer.

The manufacturing process is simple and scalable, materials are inexpensive and easily available.

3.0 Mechanics Of Bilayers

In this chapter, we analyzed the effects of unloading threshold and sample geometry on the resulted bending, which is measured by the curvature. Firstly, a single layer of each individual material was tested, and the resulting data was combined and compared with that of the composite. Then the bilayer with different width and aluminum thickness data are shown. The effect of large strain and end constraints are discussed at the end.

3.1 Tensile Behavior Of Individual Layers

The mechanical properties of polymer were assessed by stretching a single layer of 8 mm width. The loading-unloading response of the polymer at various unloading thresholds is illustrated in Fig. 9. Initially, the stress increased linearly as the strain increased, and the sample almost fully recovered its original length upon unloading. However, once the stress exceeded approximately 25 MPa, the polymer experienced permanent deformation. This permanent deformation is recorded by subtracting the strain during loading from the strain during unloading at the same force threshold, 0.5 N.

The relation of permanent deformation and maximum strain applied of the polymer is shown in Fig. 11 with blue circles. The sample can be considered as an elastoplastic material, with a modulus prior to yield of 1.3 GPa and a yield strength of roughly 25 MPa.
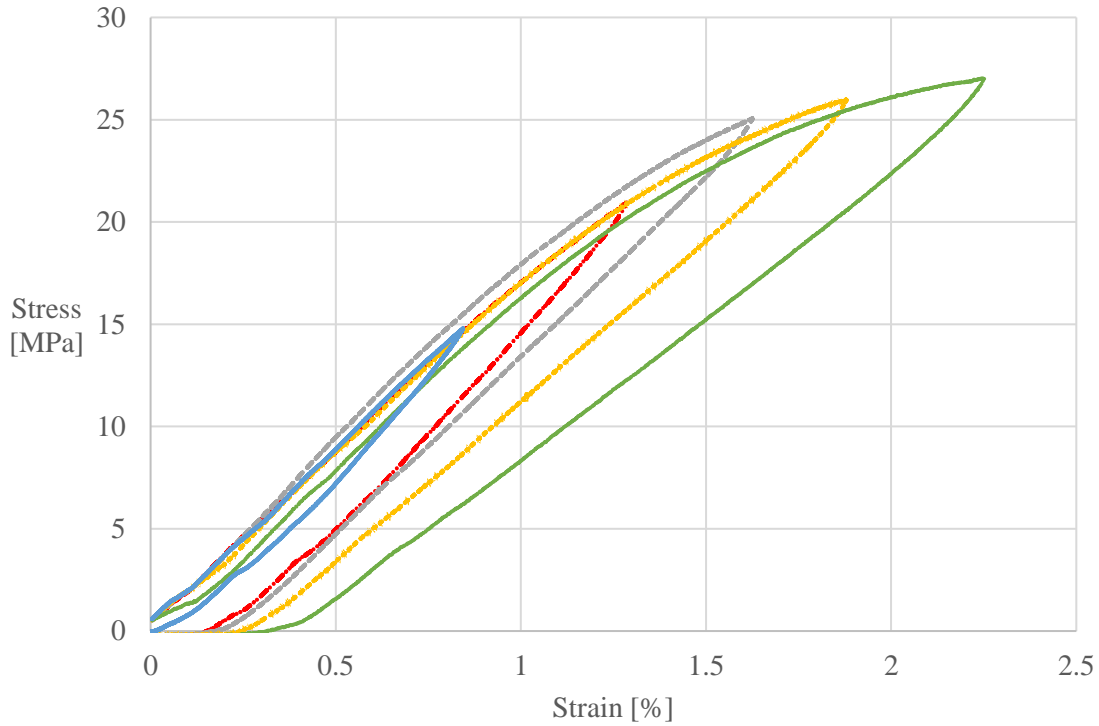
Figure 9: Stress-strain curves of single layer polymer strips with different unload thresholds.

Identical experiments were carried out on the aluminum layer; however, it can only be done at a thickness of 50 μm and higher since thinner foils tend to crumple easily when mounted onto the tensile grips at smaller thicknesses. The stress-strain data obtained at a thickness of 50 μm are presented in Fig. 10. Supplier's data shows that the aluminum has a yield strength of 17.2 MPa, which is slightly lower than our estimate of approximately 25 MPa. The initial stress strain curve allows a modulus of 20.6 GPa, which is far lower than the expected value of 270 GPa of aluminum. We are uncertain of the discrepancy, but in light of small displacement, it may be due to instrument compliance. Upon unloading, the aluminum returns to its initial form to some extent. The black line illustrated the permanent strain, calculated by subtracting the strain during unloading to the strain during loading at 0.5 N. The permanent strain of aluminum is depicted in Fig. 11 using open red squares for 50 μm and black triangles for 100 μm. The grey line depicted

16

perfect plastic, which is close to the aluminum data, indicating there is little recoil in the

aluminum layer.
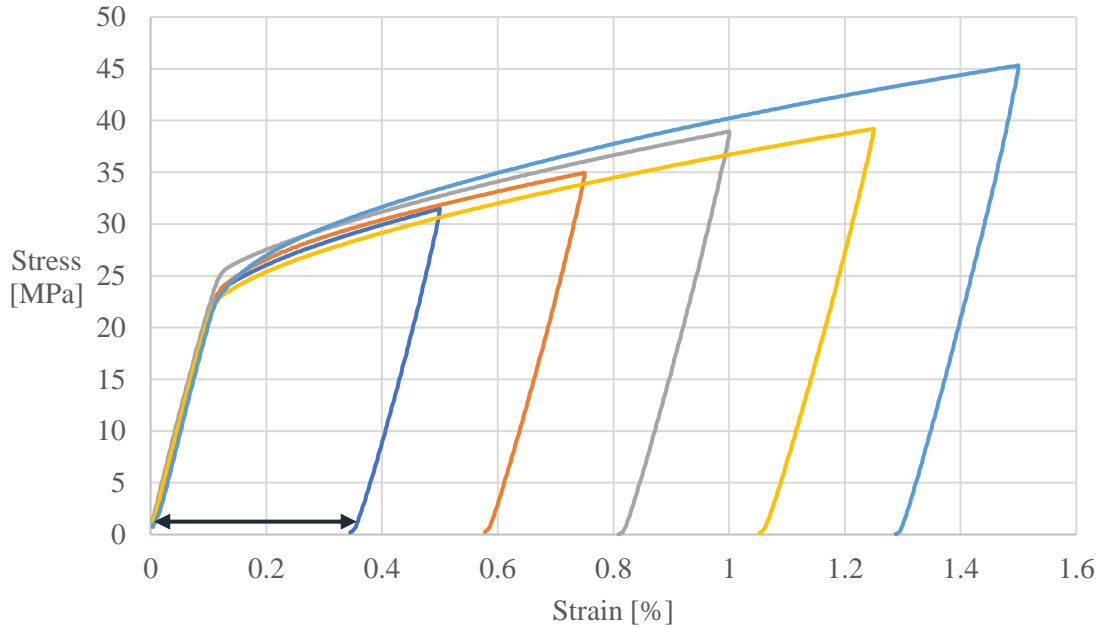
Figure 10: Stress-strain curves of aluminum strips with different unload thresholds.
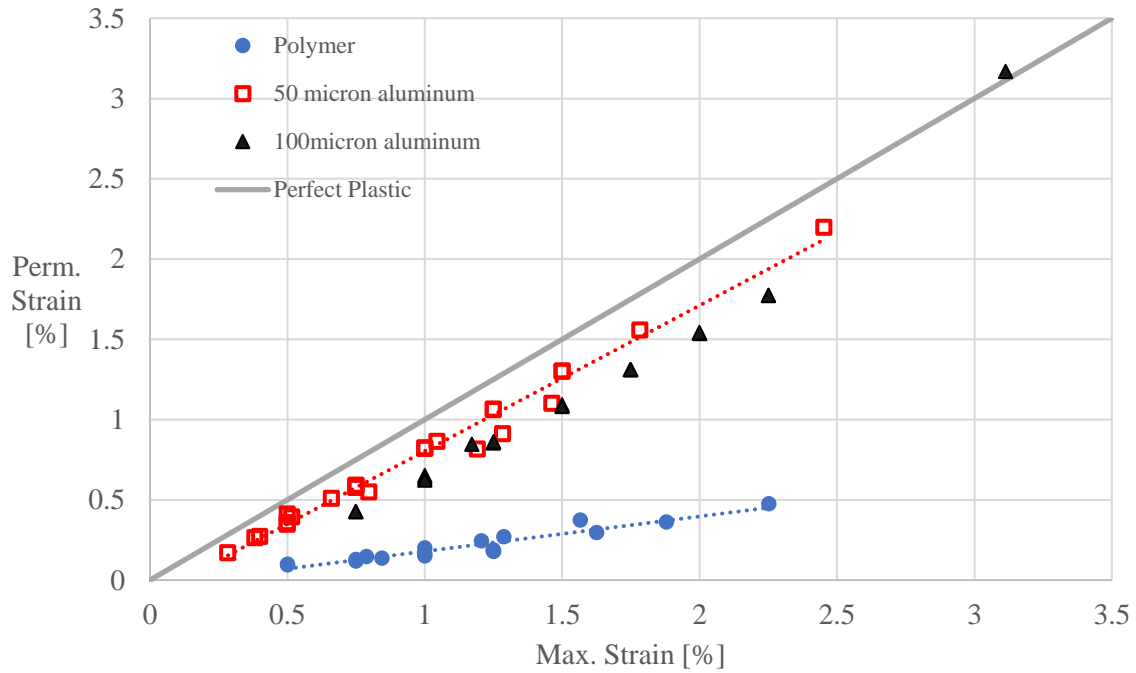
Figure 11: Permanent strain vs. Maximum strain of polymer and aluminum.

When a bilayer is stretched to a specific strain, both layers undergo the same amount of strain. Therefore, the difference between the aluminum and polymer's permanent deformation can be approximated as the strain mismatch. This strain mismatch can be calculated by fitting each layer's dataset to straight lines and subtract the polymer from aluminum:

$$\epsilon_m = 0.7\epsilon_{max} - 0.125. \tag{3.1}$$

However, it is challenging to measure the permanent strain of the polymer with the maximum strain less than 1%, so this equation will only be used to compare with strain mismatch estimation from previous theory of bilayers.

3.2 Tensile Behavior Of Bilayer

This section will discuss aluminum-polymer layered composites. Figure 12 shows an example of load-displacement curve for the bilayer different aluminum thickness, along with that for a layer of polymer alone with the same unload threshold.

During unloading, the composite force gradually reduces to almost zero at a considerable non-zero displacement, indicating that the composite undergoes permanent deformation. On the right side of Fig. 12 are examples of a bilayer sample after unloading.

18
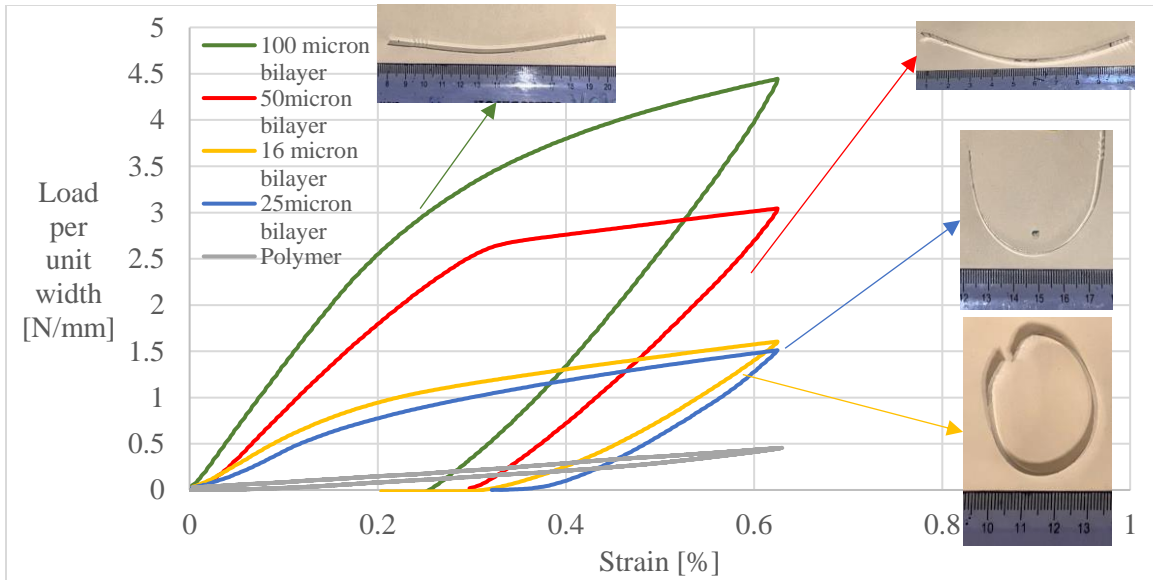
Figure 12: Load-Unload curves of bilayer and polymer.

When subjected to higher strain, as expected, the bilayer permanent deformation, or permanent strain increases, shown in Fig. 13. The width of the sample can influence this relationship, with the wider sample having slightly smaller permanent strain compared to a narrower sample. This may be related to delamination, which will be discussed later in Section 3.3.2.
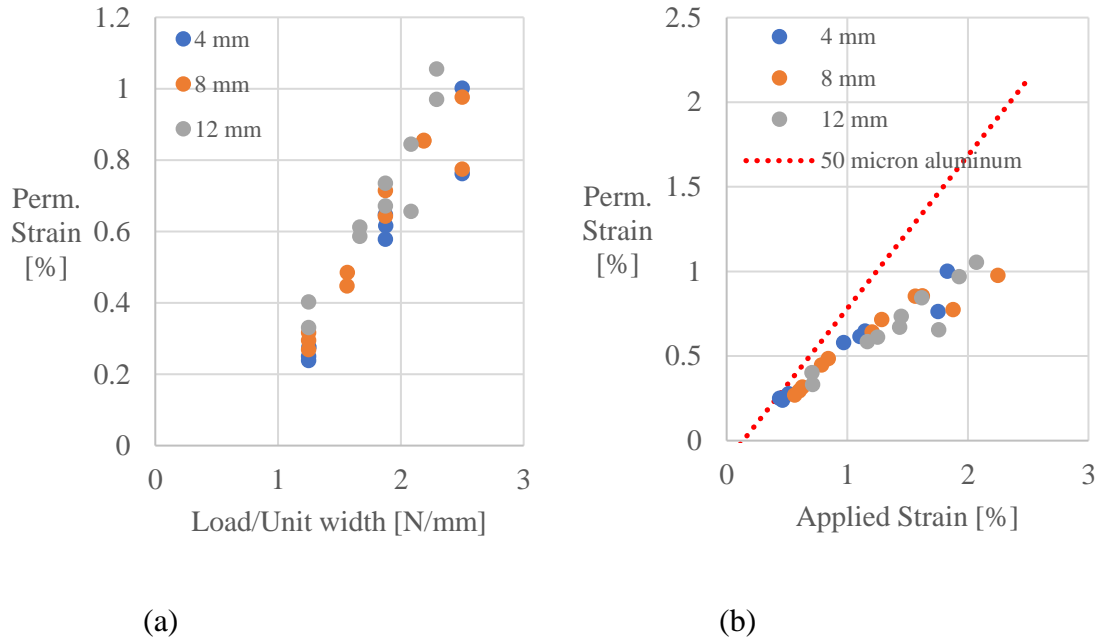
Figure 13: Permanent strain of 16 micron aluminum bilayer with different width. (a): Permanent strain vs. load per unit width. (b): Permanent strain vs. maximum strain.

The permanent strain is insensitive to the thickness of aluminum: at the same maximum applied strain, the permanent strain is nearly independent of aluminum thickness for the same grade of aluminum from McMaster-Carr, as seen in Fig. 14. We expect that the permanent strain of the bilayer should lie between those of aluminum and polymer, and since the modulus of aluminum is much larger than of the polymer and the two layers have comparable thickness, it is also expected that the permanent strain of the bilayer should be closer to the aluminum. The permanent strain can be observed to increase linearly in tandem with the maximum strain.
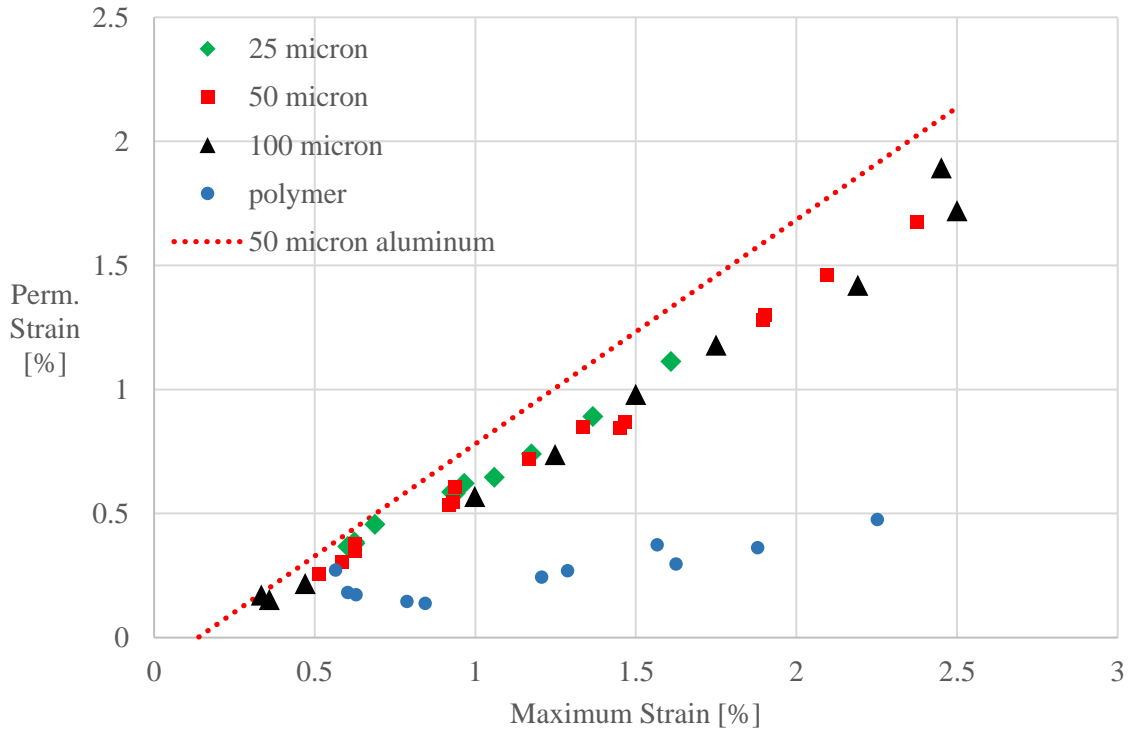
Figure 14: Permanent strain of bilayer with different aluminum thicknesses.

3.2.1 Layer Contributions

We used a subtraction method to calculate the contribution of aluminum in the bilayer and compare it with data from aluminum alone, presented in Fig. 15. On the left side, the green curve illustrates the aluminum contribution in a 50 μm aluminum bilayer by subtracting the polymer force from the bilayer. This force data then was converted to stress-strain, as shown on the right side, which agrees well with the 50 μm aluminum. This agreement means that the force contribution of each layer in the bilayer is additive, as may be expected since they experience the same strain during loading.

(a)   (b)
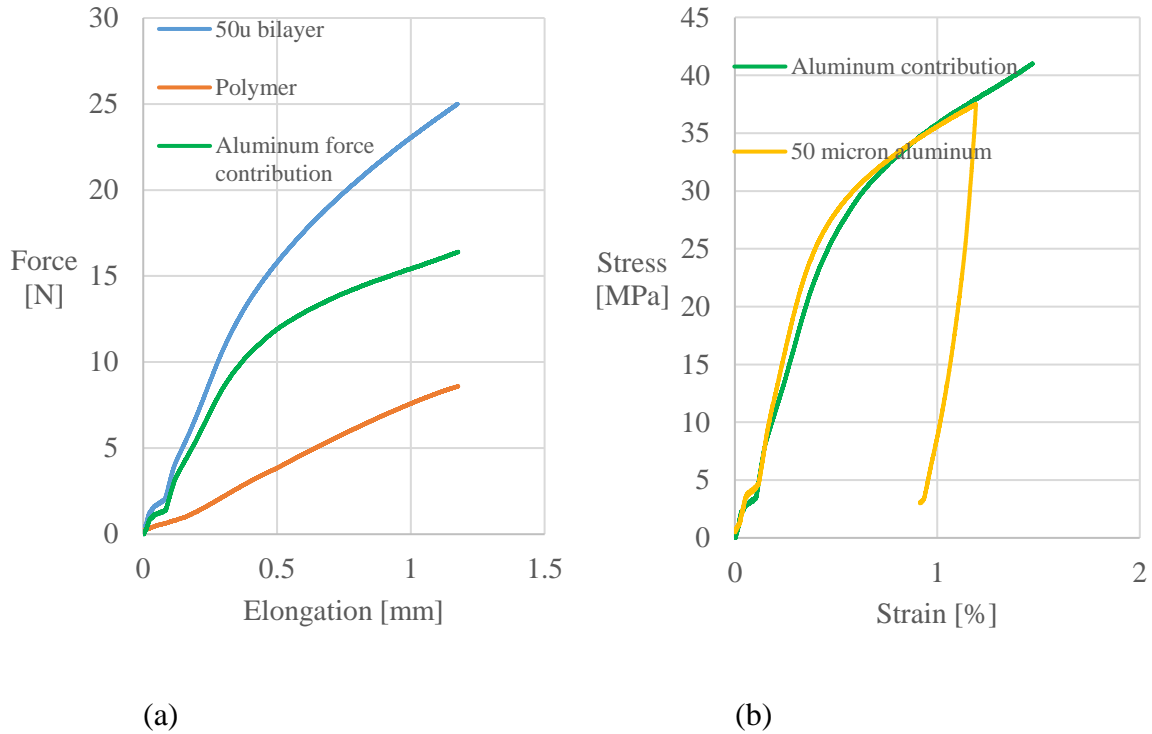
Figure 15: (a): Aluminum force contribution derived from bilayer and polymer; (b): comparison of force contribution and strip of aluminum sample.

3.3 Permanent Strain And Curvature Of Bilayers

Figure 16 show examples of 16 μm aluminum bilayer samples with different width released from the same load per width. The curvature estimated from these images is shown in Fig. 17. Wider samples exhibit slightly lower curvatures considering the same strain applied. At high strain, these samples show delamination of the aluminum layer. The curvatures of these samples plotted in Fig. 17 were measured from samples that were unclamped suddenly from maximum strain. We will discuss this in greater detail in Section 3.3.2.

The curvature rises considerably as the strain is applied, however, after reaching approximately 2% strain, the curvature of the bilayer becomes non-uniform. The bilayer develops

22

a noticeable ridge in the middle while the adjacent region flattens. This phenomenon will be examined in greater detail in Section 3.3.2.
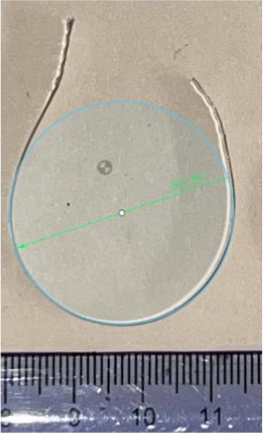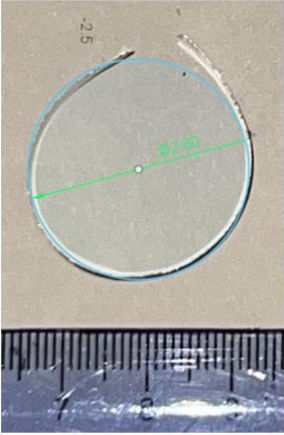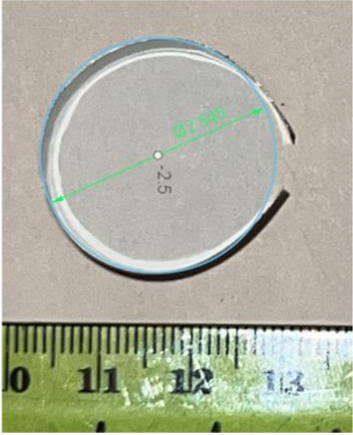
Figure 16: Curvature of aluminum bilayer of different widths at the same load per unit width of 1.875N/mm.
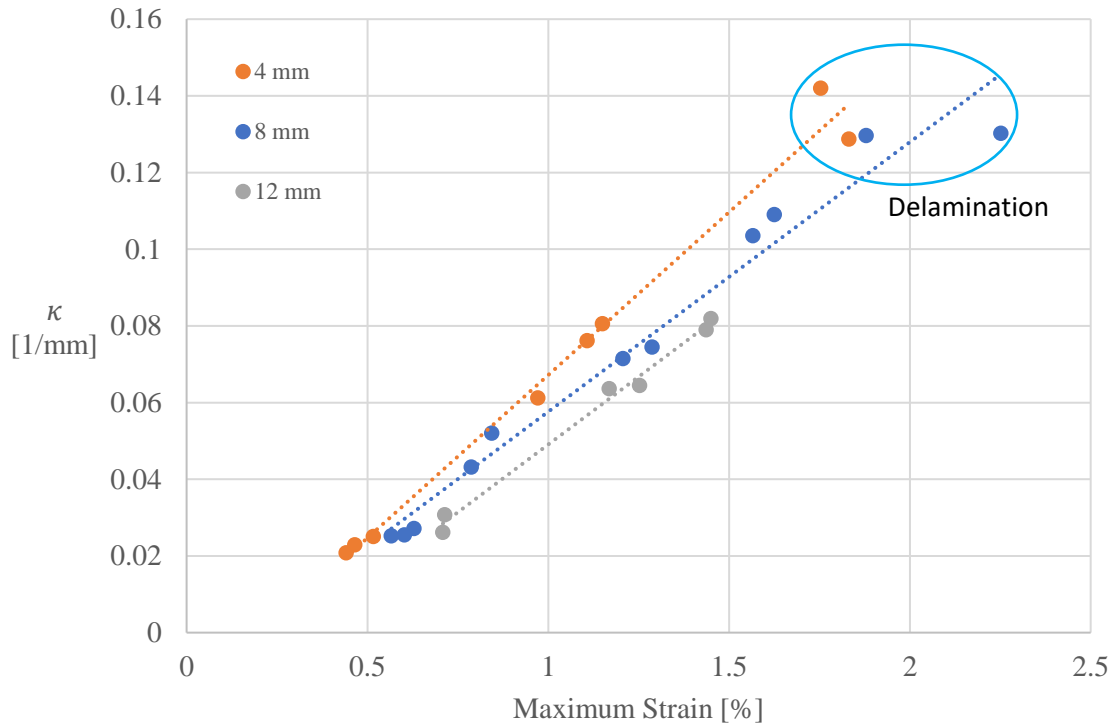
Figure 17: Curvature of bilayer with different sample width.

The aluminum thickness has a heavy influence on the outcome of the curvature, as shown in Fig. 18. Going from 25 μm to 50 μm aluminum, the curvature reduces from 0.055 mm^{-1} to 0.025 mm^{-1} at about 1% applied strain, while the curvature of the 100 μm aluminum bilayer at the same level of applied strain is only 0.003 mm^{-1}. This was anticipated by Fig. 4.
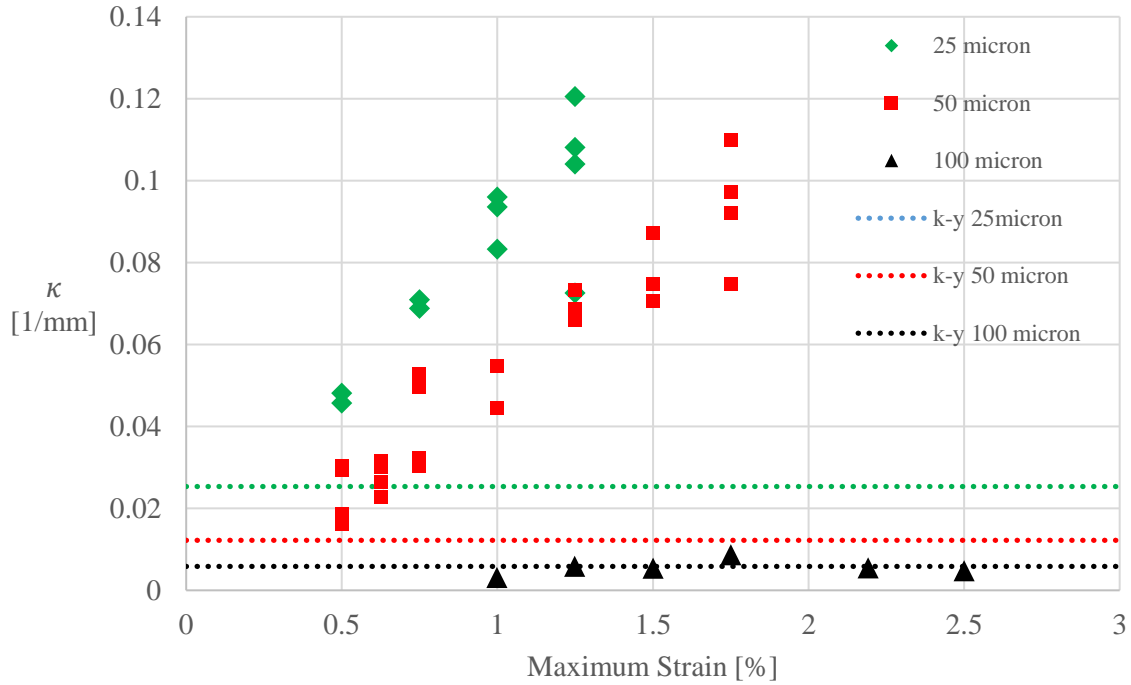
Figure 18: Curvature of bilayer with different aluminum thicknesses.

Dashed lines in Fig. 18 indicated κ_Y calculated from Eq. (1.5). Since the curvatures exceed κ_Y, it is possible that the aluminum layer may be yielding in compression after being released. Some back-of-the-envelope calculations may be used to compare the stress experienced by the aluminum against its yield stress. The tensile yield strength provided by the supplier, 17.2 MPa, is assumed to be also yield strength in compression (indeed our tensile experiments shown above in Fig. 10 suggest a yield strength of less than 25 MPa). Ramachandran et al. (2021) showed clear experimental evidence that the plastic layer in rubber-plastic composites yields in compression upon release, and that is possible for the metal-polymer bilayer system for the aluminum layer. At 1% applied strain, the polymer can be assumed to impose a maximum force of

$$(1.3 \text{ GPa}) \text{ x } (0.01) \text{ x } (50\text{E-6 m}) \text{ x } (8 \text{ mm}) = 5.2 \text{ N}.$$

to the aluminum. This implies the corresponding stress to an aluminum layer of 50 μm to be:

$$(5.2 \text{ N}) / (8 \text{ mm}) \text{ x } (50\text{E-6 m}) = 13 \text{ MPa}.$$

25

This is too low to induce yielding, even though the curvature results exceed the value needed for partial yield. The above calculation assumes that polymer is perfect elastic and aluminum is perfect plastic, however they both have some elastic recovery, indicating that the threshold for yielding of aluminum must be higher. Thus, Eq. (1.5) is inadmissible for this system, and a method to capture yielding of aluminum during release remains to be pursued. For the smaller thickness aluminum however, this force will impose a stress of

$$(5.2 \text{ N}) / (8 \text{ mm}) \text{ x } (16\text{E-6 m}) = 40 \text{ MPa}.$$

on the 16 μm aluminum layer, which may make it to yield.

3.3.1 Comparison With Fully-Elastic Theory

By back calculating the strain mismatch from the measured curvature, Fig. 19 shows the estimation of required strain mismatch to get a set value of curvature, based on Eq. (1.4), in blue circles. The yellow lines indicate Eq. (3.1), which represents the difference in permanent strain of aluminum and polymer. While the 25 μm results are in reasonable agreement with the estimated strain mismatch as seen in Fig. 19a, the 50 μm results are puzzling since the mismatch required to reach the observed curvature is higher than the estimated mismatch. In principle this should not be possible since Eq. (3.1) should be the highest strain mismatch available. One possibility for this is that the adhesive layer may play a role.

To account for the additional layer of adhesive in our bilayer system, we treat the adhesive's elastic modulus as negligible and estimate the resulted curvature from strain mismatch with the introduction of adhesive thickness h_a:

$$\kappa = \frac{6\epsilon_m(2h_a + h_f + h_s)}{\dfrac{h_f^3}{h_s}\dfrac{E_f}{E_s} + \dfrac{h_s^3}{h_f}\dfrac{E_s}{E_f} + 12h_a(h_a + h_f + h_s) + 4(h_f^2 + h_s^2) + 6h_f h_s} \tag{3.2}$$

Equation (3.2) was derived by a fellow researcher, Fatemeh Rouhani (unpublished) and crosschecked against finite element analysis conducted in ABAQUS. Figure 19a shows that if we use Eq. (3.2) to estimate the strain mismatch from the curvature, the corresponding values do not change significantly. Thus, the presence of the adhesive does not seem to be the reason for the discrepancy between the strain mismatch estimated from the curvature vs. Eq. (3.1). The required strain mismatch for our bilayer system, technically a trilayer, is higher than that of a classic bilayer system.

(a)   (b)
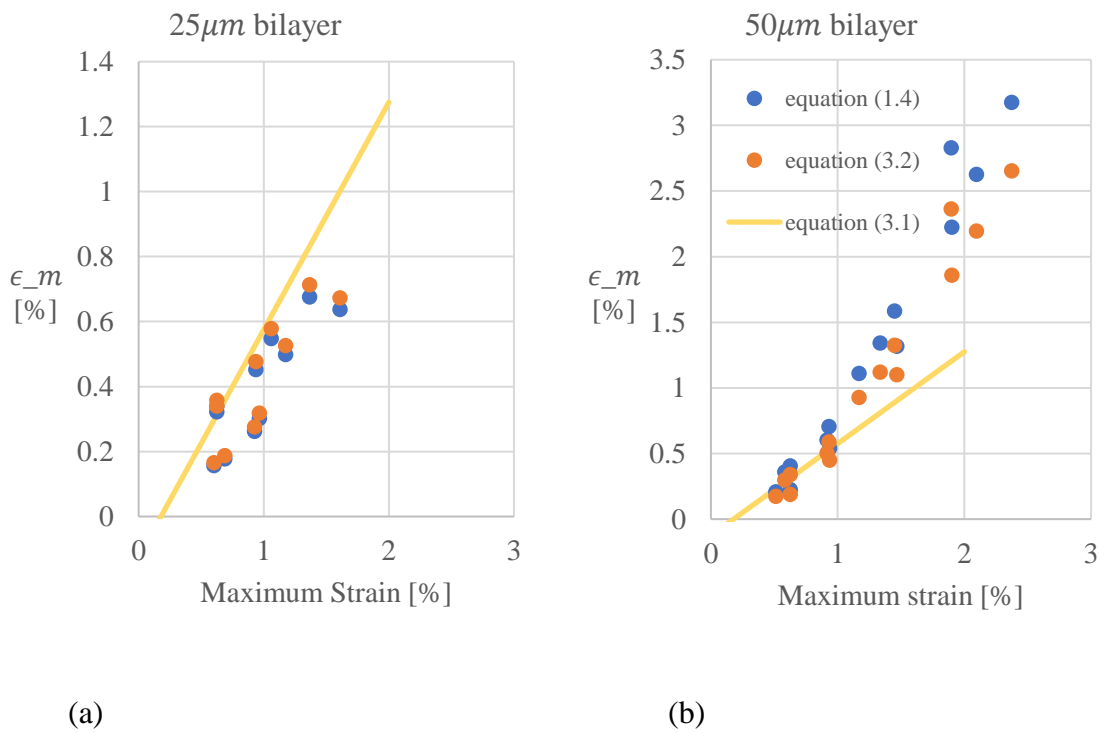
Figure 19: Comparison of required strain mismatch between classic bilayer theory, adjusted equation with inclusion of adhesive, and measured data. (a): 25 micron bilayer. (b): 50micron bilayer.

3.3.2 Sudden And Slow Release

In bilayers with small aluminum thickness, at high strain typically above 2%, when released slowly while still being clamped, the bilayer forms a ridge, examples shown in Fig. 20. On another hand, when the sample is suddenly released from the maximum strain, this phenomenon would not happen. Figure 21 shows detailed views of these ridges.
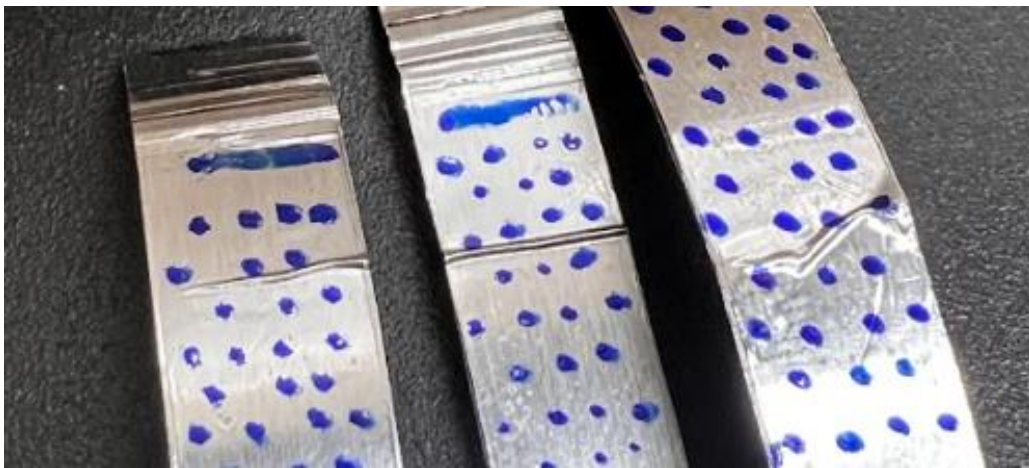
Figure 20: Ridges formed at high maximum strain.
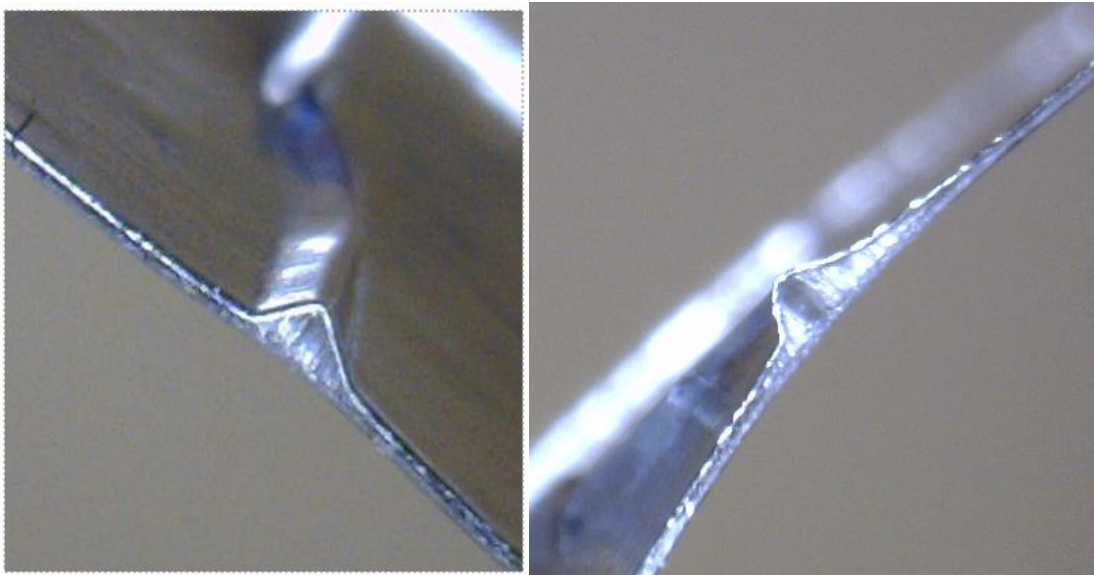
Figure 21: High magnification views of ridges.

A bilayer has many ways to relieve strain mismatch. These include stretching or compressing the layers in-plane, bending out of plane, wrinkling, delaminating, and forming helical shapes if there are end-constraints. In systems that allow for permanent deformation, any of these methods may be accompanied by plastic deformation. Another pathway to relieve strain mismatch is the formation of ridges, which is available to systems with a highly compliant layer between the two layers. If one of these pathways is facilitated, it will be preferred over the others. Conversely, if most of these pathways are eliminated, the remaining pathway will be the only one available. To verify this, the same experiment was repeated, but with a sudden release at the maximum strain. The ridges did not appear in this case, and the sample developed a uniform curvature like similar samples at smaller maximum strain. This supports the notion that the formation of ridges occurs because during the gradual unloading process, the system is prevented from undergoing bending, stretching in-plane, and twisting.
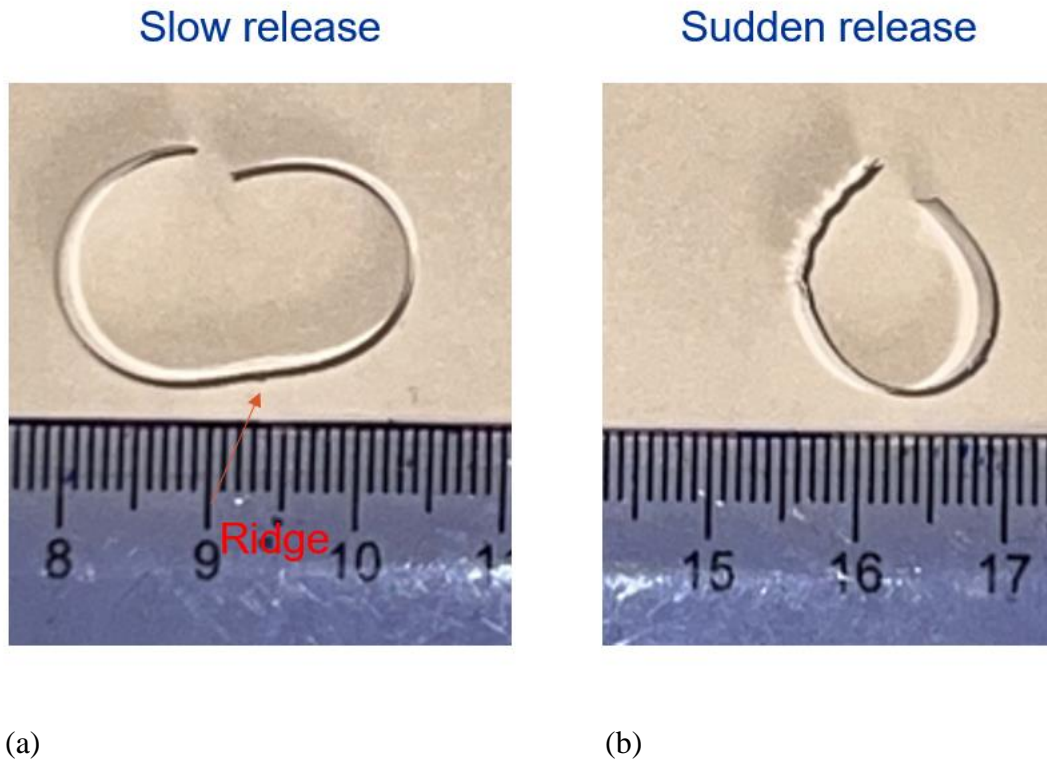
Figure 22: Comparison of curvature between slow and sudden release. (a): sample that was unloaded while still being clamped. (b): sample that was unloaded suddenly from maximum strain.

Figure 22 shows the comparison between unclamping after unloading vs. unclamping suddenly while the sample is at maximum strain. The samples were trimmed after testing to avoid overlapping of the edges. We can see that the sample that was unclamped suddenly has a larger curvature than the sample that was unloaded before unclamping due to higher strain mismatch energy. On samples that were unloaded before clamping, part of this energy has transferred to the ridge, hence a smaller curvature.

During our observations, we noticed that delamination occurred in the 16 and 25 μm aluminum bilayer samples. However, this phenomenon did not occur in thicker aluminum bilayer samples. Nonetheless, it is possible that delamination may occur at high strain in the thicker aluminum bilayer samples, but our equipment is not capable of reaching such high strains.

30

To summarize, in this chapter, we found that the curvature that determines the bending level can be controlled by changing the composite strip's geometry and layer thickness, as well as unloading threshold. The classic theory that is based on energy minimization method proved to be working under the assumption that the adhesive layer has negligible modulus and below a certain thickness ratio. At high strain and small thickness ratio between the aluminum and the polymer, when released slowly from being clamped, the composite strip will form a ridge and reduce the resulting curvature.

4.0 Patterned Bending

From the understanding of the deformation-induced bending of the bilayer, we can now target specific shape by localizing the bending and control the bending direction and level. Figure 23 shows an example of a W shape that may be generated from a trilayer with a sequence of defects when the trilayer is subjected to stress and then released.
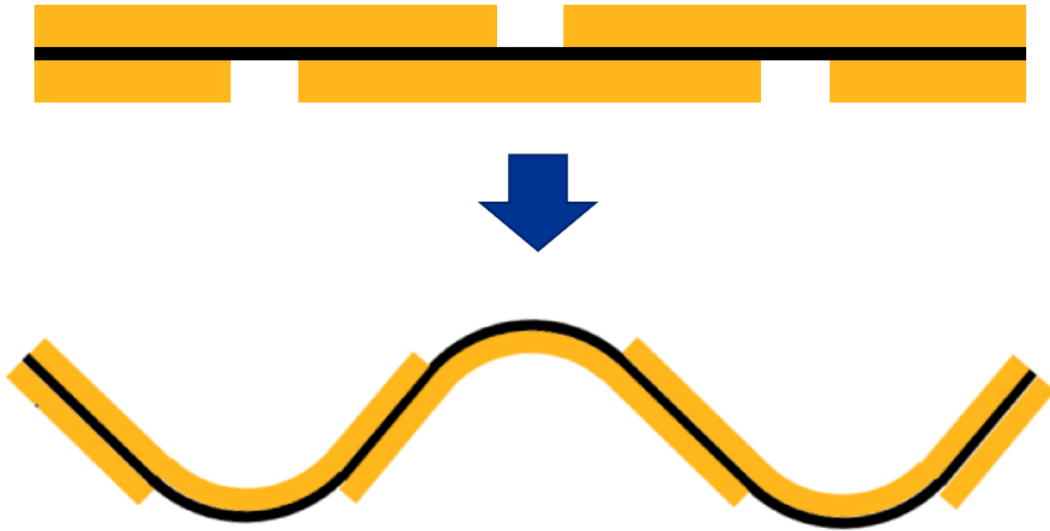
Figure 23: Schematic example of trilayer with a defect sequence to generate a targeted shape.

The approach taken here is to construct trilayers using the same procedure as above. We can then remove selected areas from the trilayer using laser and thereby creating regions that are bilayers, These regions where one of the polymer layers is removed are named trenches henceforth. Fig. 24 shows a simplified schematic to illustrate this method. Upon stretching and releasing, the regions in the trenches bend, whereas the intact trilayer regions remain straight. These regions still have a strain mismatch between the aluminum and polymer layers, but they are symmetric and hence do not bend. Since all defects in the strip experience the same force (not the same strain),

the experiments were conducted by loading to some target force and then unloading. In contrast, in the previous chapter, samples were loaded to a target strain. The trench angle is the angle between the trench direction and the direction of stretching, illustrated in Fig. 25. In this project, 90° and 45° trench angles were examined. After stretching and release, samples were laid on the side and photos were taken from a far distance to reduce optical distortion. To achieve the maximum amount of bending, 16 μm aluminum is selected for these experiments.
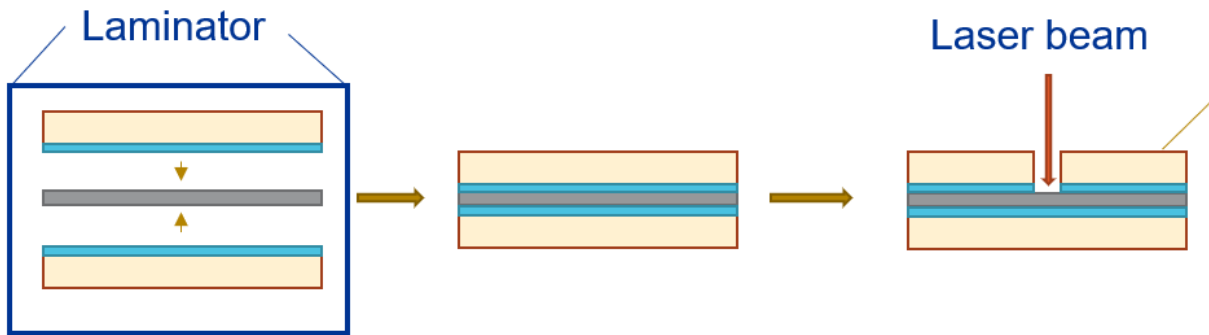
Figure 24: Manufacturing of trilayer with trench.

Figure 25: Properties of trench and definition of bending angles.

4.1.1 90° Trench

To quantify the behavior of 90° trenches, different input parameters were varied, and the external bending angle was measured and plotted as output in Fig. 26 and 27. With the same trench

width of 2 mm, this angle increases with increasing load threshold, and beyond approximately 14 N, it can reach over 180°, shown in Fig. 26. Figure 27 shows examples of the resulted bending: the bending can vary from gentle to strong – beyond 180°.

In Fig. 28, under the same maximum load of 10 N, external angle increases with trench width gradually. Figure 29 shows the reproducibility of the external angle, recorded from samples of 3 mm trench width at 10 N.
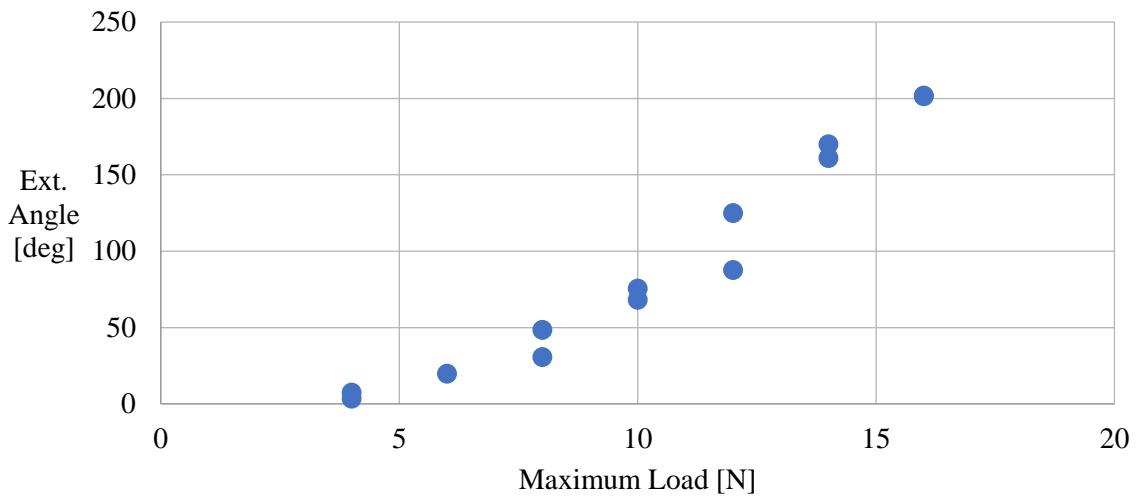
Figure 26: External angle of trilayers with 90° trench and 3 mm trench width with different unloading threshold.

(a)   (b)
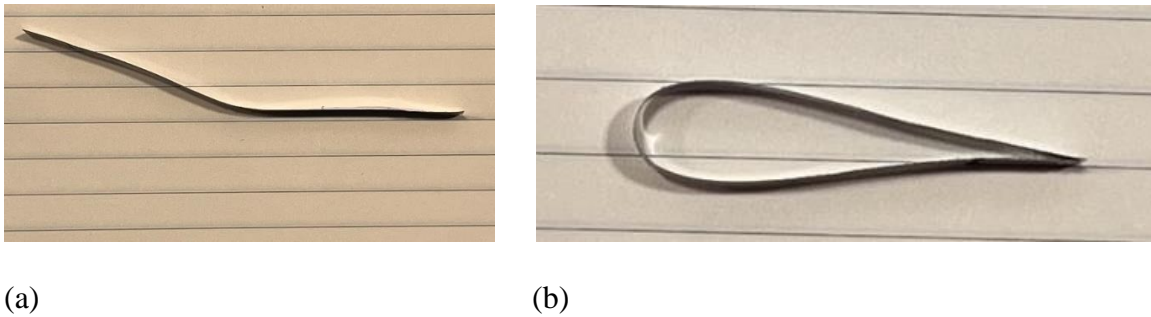
Figure 27: Example of 8 mm wide trilayer with 10 mm 90° trench after stretch and release at different unloading threshold. (a): 6 N - 19.7° external angle. (b): 16 N - 201.7° external angle.
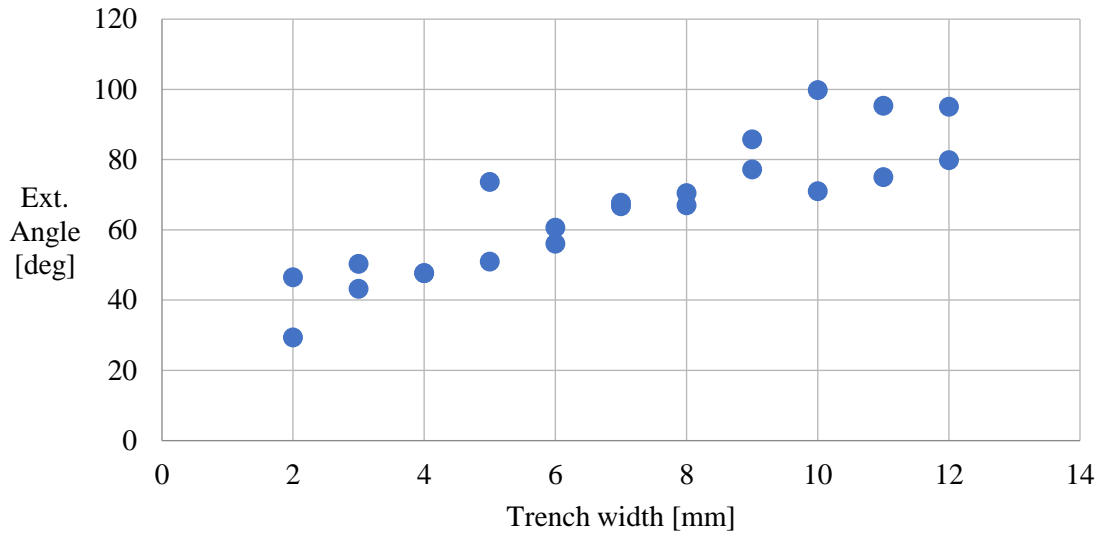
Figure 28: External angle of trilayers with 90° trench unloaded from 10N with different trench width.
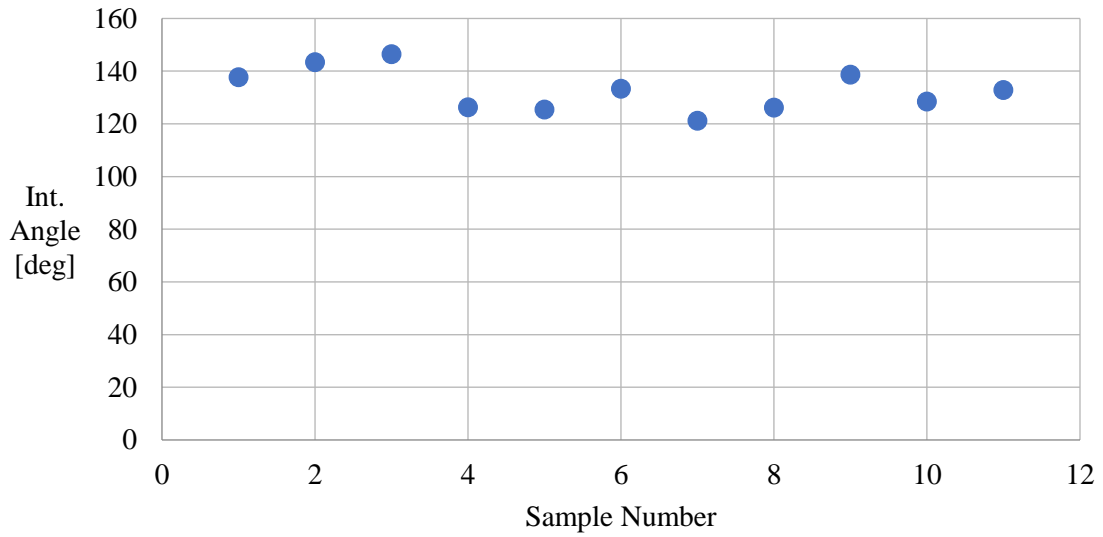
Figure 29: Internal angle of trilayers with 3 mm 90° trench unloaded from 10 N. Each point denotes an independent sample to illustrate the degree of variability.

4.1.2 45° Trench

To generate out of plane bending, 45° trench trilayer was stretched and released. Note that angled trenches imply a gradient in strain across the width of the sample and hence strictly, it is not possible to treat the strain in the sample as varying only along the width direction. Different trench width as well as different unload threshold was tested. To create a helix shape, 200 mm long samples with 2 mm 45° trenches span across the whole clamp-to-clamp distance, with the spacing between trenches varying, were tested. Figure 31 shows examples of such helixes seen from the side. Photos were taken with samples submerged in water to reduce the effect of gravity on the samples so that the 3D shape of the sample is less affected by gravitational sagging. The resulting pitch and diameter are shown in Fig. 30.
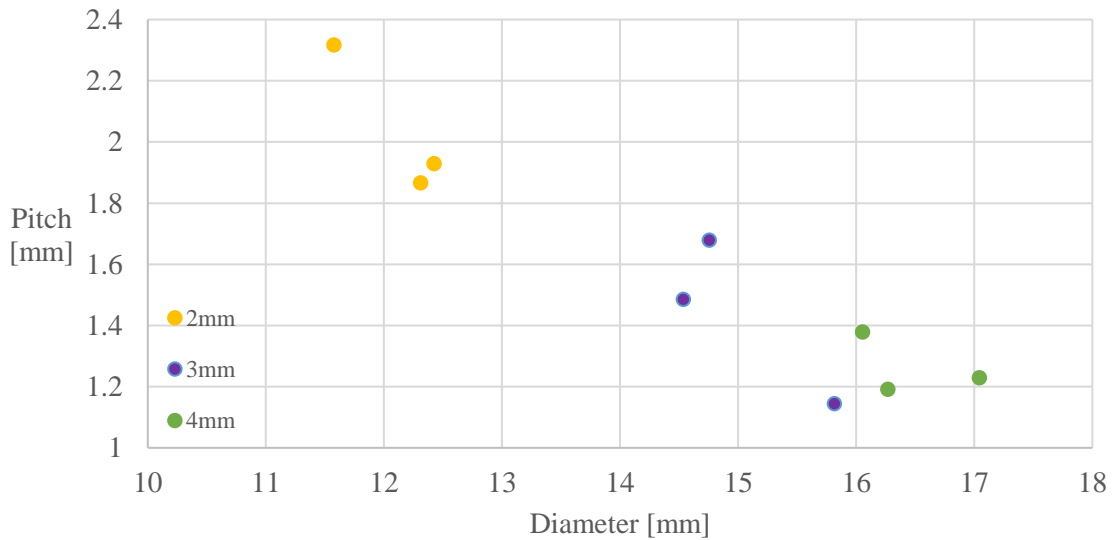
Figure 30: Pitch and diameter of helix with 45° trenches with different trench spacing.

(a)

(b)
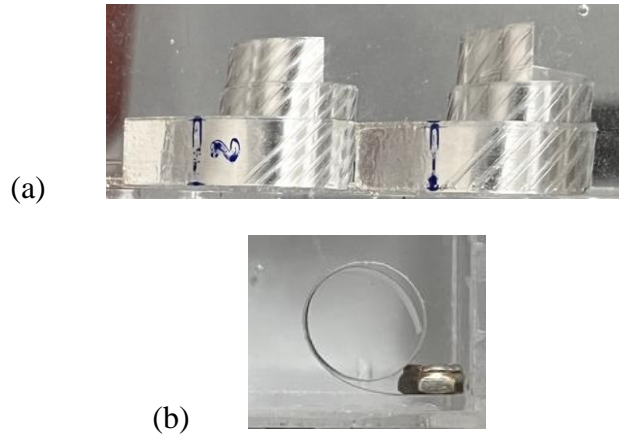
Figure 31: Examples of helixes formed from trilayer with multiple 45° trench and different spacing. a:pitch measuring - left: 2 mm spacing, right: 3 mm spacing. b: diameter measuring.

4.1.3 Lantern-Like Shape

We will now illustrate the potential use of aluminum-polymer laminate to create structures using self-folding origami principles. A possible shape that can be created with simple technique is a lantern. Wide bilayer sample with long slit cutout, as shown in Fig. 32, can be pulled in a straight configuration, or bonded to a cylinder block then pulled to make a lantern. The first method proved to be easier, although it proved somewhat difficult to maintain a uniform stress across the width of the sample. The second method, which is to bond the wide sample to a cylinder block, is difficult to get all sections of the bilayer level. The author seeks to improve the technique with the use of 3D printing to make fixtures that can self-balance to maintain a uniform stress across the sample.

Figure 32: Lantern-like shape formed from wide bilayer with long slit cutouts.

5.0 Summary And Future Directions

Self-folding origami has become a popular area of research due to its potential application in various engineering fields, including architecture, soft robotics, and biomedical devices. This thesis aims to explore the deformation-induced shape morphing that results from the interplay of plastic and elastic deformation in bilayer and trilayer systems. To facilitate this investigation and potential applications, a simple and cost-effective method is developed to create samples using inexpensive and robust materials. Tensile stretch-release experiments are conducted on bilayers of aluminum and polymer laminating films to investigate their bending behavior under various conditions.

By comparing the summation of individual layer's force responses with the bilayer composite, we found that they contribute to the total force response additively. Quantitative analysis of permanent strain and curvature opens the ability to program the bending.

The aluminum-polymer bilayer composite readily bends in response to deformation-induced strain mismatch by stretch and release. Curvature realized from aluminum-polymer bilayer increases with the applied load (or equivalently the strain applied before unloading). The curvature was found to be insensitive to sample width and found to reduce with increasing aluminum layer thickness. All these results are consistent with expected from established theory for fully elastic bilayers. In this project, for maximum strain value in range from 0.5% to 2%, bilayers can produce curvature from 0.02 to $0.14\ mm^{-1}$ for the polymer-aluminum bilayers using $16\ \mu m$ aluminum foil. Thus cm-scale radius of curvature can be reached readily from such bilayers. However, at small aluminum thickness and high strain, aluminum-polymer bilayer can develop ridge due to delamination and reduces the resulting curvature.

One important question posed at the outset is whether the aluminum layer would yield under compression during unloading. On this question, the results are inconclusive. On one hand, the stress induced by the polymer layer during unloading is estimated to be much smaller than the required stress to force the aluminum layer to yield. On the other hand, the measured values of curvature exceed the values for partial yielding of the aluminum as predicted by Suresh et al. (1994)

Patterned bilayers were made possible by using a laser cutter to remove trenches from trilayer polymer-aluminum-polymer laminates. Trilayers do not bend since they are symmetric, but the regions of laser-induced damage become asymmetric similar to bilayers thus inducing bending when stretch-released. Simple trench angles were examined, and the result bending measured. With the goal of pre-programming long ribbons to bend into complex 3D shapes, we show that a helix shape can be generated by stretching trilayer with a sequence of tilted trenches. The helix's pitch and diameter can be controlled by varying trenches' spacing and width. When considering post-processing, possibilities include lantern-like objects by stretching wide bilayer sample with slit cutouts.

5.1 Future Work

There are several challenges encountered during this project. Although the curvature as the result of deformation-induced strain mismatch in a bilayer can be captured quantitatively, an analytical model to calculate the strain mismatch and curvature from applied strain remains a challenge. An approach to this matter is using finite element analysis, where material's properties like elastic modulus, yield strength/strain, strain hardening may be varied independently.

The second challenge involves understanding the role of the adhesive in the possibility of aluminum yielding during unloading. For most of this thesis, the aluminum polymer composites are treated as if they were bilayers. In reality however, they are separated by a layer of adhesive whose thickness is not negligible – indeed in some cases, it exceeds the thickness of the aluminum itself. A thorough investigation of the adhesive's role is necessary to develop a precise model.

The third challenge pertains to trilayer regions in a trilayer with trenches that show significant out-of-plane bending outside the trench despite being assumed to be symmetric. Deformation in the adhesive layer may be responsible for this. However, trenches at various angles, including 45°, do not show much out-of-plane bending in comparison to a trenched trilayer made from scotch tape and aluminum, which reduces the versatility of this approach for realizing complex 3D shapes from patterned ribbons. This issue needs to be addressed in future work. In contrast, we found that a bilayer of scotch tape and aluminum behaves more in accord with expectations. For instance, tilted trenches induce bending that follows the tilt direction almost faithfully. Moreover, even when heated, the curvature changes are expected, with the aluminum being on the concave side as expected from its lower thermal expansion coefficient. Upon heating above the melting point of the scotch tape, the curvature changes sign and stays permanently changed due to irreversible shrinkage of the scotch tape layer. This finding raises the question of whether the aluminum-polymer bilayer system behaves similarly when the strain mismatch is induced thermally which can also be investigated.

Bibliography

1, Xyron 9" ezLaminator. Retrieved from https://www.xyron.com/p/professional-machines/ezlaminator/ezlaminator-624672/

2, Stoney, G. G. (1909). The tension of metallic films deposited by electrolysis. *Proceedings of the Royal Society of London. Series A, Containing Papers of a Mathematical and Physical Character, 82*(553), 172-175.

3, Myer, J. H., & Cooke, F. (1969). Optigami—A tool for optical systems design. *Applied Optics, 8*(2), 260-260.

4, Suresh, S., Giannakopoulos, A., & Olsson, M. (1994). Elastoplastic analysis of thermal cycling: layered materials with sharp interfaces. *Journal of the Mechanics and Physics of Solids, 42*(6), 979-1018.

5, Smela, E., Inganäs, O., & Lundström, I. (1995). Controlled folding of micrometer-size structures. *Science, 268*(5218), 1735-1738.

6, Judy, J. W., & Muller, R. S. (1997). Magnetically actuated, addressable microstructures. *Journal of Microelectromechanical systems, 6*(3), 249-256.

7, Freund, L. B., Floro, J., & Chason, E. (1999). Extensions of the Stoney formula for substrate curvature to configurations with thin substrates or large deformations. *Applied Physics Letters, 74*(14), 1987-1989.

8, Konings, R., & Thijs, R. (2001). Foldable containers: a new perspective on reducing container-repositioning costs. *European journal of transport and infrastructure research, 1*(4).

9, Freund, L. B., & Suresh, S. (2004). Thin film materials: stress, defect formation and surface evolution. In: Cambridge university press.

10, Tremblay, E. J., Stack, R. A., Morrison, R. L., & Ford, J. E. (2007). Ultrathin cameras using annular folded optics. *Applied Optics, 46*(4), 463-471.

11, ToolBox, E. (2008). Aluminum Alloys - Mechanical Properties. Retrieved from https://www.engineeringtoolbox.com/properties-aluminum-pipe-d_1340.html

12, Tachi, T. (2010). *Geometric considerations for the design of rigid origami structures.* Paper presented at the Proceedings of the International Association for Shell and Spatial Structures (IASS) Symposium.

13, Wu, W., & You, Z. (2011). A solution for folding rigid tall shopping bags. *Proceedings of the Royal Society A: Mathematical, Physical and Engineering Sciences, 467*(2133), 2561-2574.

14, Sreetharan, P. S., Whitney, J. P., Strauss, M. D., & Wood, R. J. (2012). Monolithic fabrication of millimeter-scale machines. *Journal of Micromechanics and Microengineering, 22*(5), 055027.

15, Kim, J., Hanna, J. A., Byun, M., Santangelo, C. D., & Hayward, R. C. (2012). Designing responsive buckled surfaces by halftone gel lithography. *Science, 335*(6073), 1201-1205. doi:10.1126/science.1215309

16, Peraza-Hernandez, E. A., Hartl, D. J., Malak Jr, R. J., & Lagoudas, D. C. (2014). Origami-inspired active structures: a synthesis and review. *Smart Materials and Structures, 23*(9), 094001.

17, Tolley, M. T., Felton, S. M., Miyashita, S., Aukes, D., Rus, D., & Wood, R. J. (2014). Self-folding origami: shape memory composites activated by uniform heating. *Smart Materials and Structures, 23*(9), 094006.

18, Na, J. H., Evans, A. A., Bae, J., Chiappelli, M. C., Santangelo, C. D., Lang, R. J., . . . Hayward, R. C. (2015). Programming reversibly self-folding origami with micropatterned photo-crosslinkable polymer trilayers. *Advanced Materials, 27*(1), 79-85.

19, Turner, N., Goodwine, B., & Sen, M. (2016). A review of origami applications in mechanical engineering. *Proceedings of the Institution of Mechanical Engineers, Part C: Journal of Mechanical Engineering Science, 230*(14), 2345-2362.

20, Janbaz, S., Hedayati, R., & Zadpoor, A. (2016). Programming the shape-shifting of flat soft matter: from self-rolling/self-twisting materials to self-folding origami. *Materials Horizons, 3*(6), 536-547.

21, Webb, D., Hirsch, B., Bradford, C., Steeves, J., Lisman, D., Shaklan, S., . . . Thomson, M. (2016). *Advances in starshade technology readiness for an exoplanet characterizing science mission in the 2020's.* Paper presented at the Advances in Optical and Mechanical Technologies for Telescopes and Instrumentation II.

22, Johnson, M., Chen, Y., Hovet, S., Xu, S., Wood, B., Ren, H., . . . Tse, Z. T. H. (2017). Fabricating biomedical origami: a state-of-the-art review. *International journal of computer assisted radiology and surgery, 12*, 2023-2032.

23, Santangelo, C. D. (2017). Extreme mechanics: Self-folding origami. *Annual Review of Condensed Matter Physics, 8*, 165-183.

24, Stern, M., Pinson, M. B., & Murugan, A. (2017). The complexity of folding self-folding origami. *Physical Review X, 7*(4), 041070.

25, Ramachandran, R. G., Hariharakrishnan, S., Fortunato, R., Abramowitch, S. D., Maiti, S., & Velankar, S. S. (2018). Necking and drawing of rubber-plastic bilayer laminates. *Soft Matter, 14*(24), 4977-4986. doi:10.1039/c8sm00684a

26, Pesenti, M., Masera, G., & Fiorito, F. (2018). Exploration of adaptive origami shading concepts through integrated dynamic simulations. *Journal of Architectural Engineering, 24*(4), 04018022.

27, Kanik, M., Orguc, S., Varnavides, G., Kim, J., Benavides, T., Gonzalez, D., . . . Fink, Y. (2019). Strain-programmable fiber-based artificial muscle. *Science, 365*(6449), 145-150.

28, Wisinger, C. E., Maynard, L. A., & Barone, J. R. (2019). Bending, curling, and twisting in polymeric bilayers. *Soft Matter, 15*(22), 4541-4547.

29, Masana, R., Khazaaleh, S., Alhussein, H., Crespo, R., & Daqaq, M. (2020). An origami-inspired dynamically actuated binary switch. *Applied Physics Letters, 117*(8), 081901.

30, Ramachandran, R. G., de Cortie, J., Maiti, S., Deseri, L., & Velankar, S. S. (2021). Uniaxial stretch-release of rubber-plastic bilayers: Strain-dependent transition to stable helices, rolls, saddles, and tubes. *Extreme Mechanics Letters, 48*, 101384.

31, Ji, J., Karna, D., & Mao, H. (2021). DNA origami nano-mechanics. *Chemical Society Reviews, 50*(21), 11966-11978.

32, Meloni, M., Cai, J., Zhang, Q., Sang-Hoon Lee, D., Li, M., Ma, R., . . . Feng, J. (2021). Engineering Origami: A comprehensive review of recent applications, design methods, and tools. *Advanced Science, 8*(13), 2000636.

33, Li, L., Long, F. L. J., Lim, I., Sun, T., & Ren, H. (2023). An Overhead Collapsible Origami-Based Mount for Medical Applications. *Robotics, 12*(1), 21.